Journal of Alloys and Compounds 524 (2012) 46–52

Contents lists available at SciVerse ScienceDirect

Journal of Alloys and Compounds

journal homepage: www.elsevier.com/locate/jallcom

Microstructures and mechanical properties of high-strength Mg–Gd–Y–Zn–Zr alloy sheets processed by severe hot rolling

C. Xu[a,b], S.W. Xu[b], M.Y. Zheng[a,*], K. Wu[a], E.D. Wang[a], S. Kamado[b], G.J. Wang[c], X.Y. Lv[c]

[a] School of Materials Science and Engineering, Harbin Institute of Technology, Harbin 150001, PR China
[b] Department of Mechanical Engineering, Nagaoka University of Technology, Nagaoka 940-2188, Japan
[c] Northeast Light Alloy Company Limited, Harbin 150060, PR China

ARTICLE INFO

Article history:
Received 24 October 2011
Received in revised form 3 February 2012
Accepted 6 February 2012
Available online 16 February 2012

Keywords:
Magnesium alloy
Hot rolling
Microstructure
Texture
Mechanical properties

ABSTRACT

Mg–8.2Gd–3.8Y–1.0Zn–0.4Zr alloy sheets containing long period stacking ordered (LPSO) phase were prepared by hot rolling at 400 °C with total reduction of 96%. Microstructure evolution of the sheets during hot rolling was investigated, and its influence on mechanical properties was discussed. Twinning occurred during the early stage of hot rolling, and disappeared after total reduction higher than 89%. Average grain size was gradually refined, microstructure became much more homogeneous and volume fraction of LPSO phase decreased with increasing rolling reduction. Furthermore, the type of LPSO phases far from and near the block shaped phases were identified to be different. Basal texture was obtained during rolling process, but the intensity declined with the further rolling, which is mainly due to the dynamic recrystallization and the addition of RE elements. The as-rolled sheet with 96% reduction shows excellent mechanical properties: yield strength of 318 MPa, ultimate tensile strength of 403 MPa and elongation to failure of 13.7% at ambient temperature along the rolling direction.

1. Introduction

In recent years, because of the low density, high specific strength, high damping capacities and good casting properties, magnesium and its alloys have been received much attention as important structural materials, and they become the focus of worldwide interest as a candidate for lightweight components in automotive, electronic and space industries [1–4]. Among various magnesium alloys, rare earth (RE) containing alloys are known to show high strength, excellent creep resistance, good thermal stability, hence, much effort has been devoted to improve the mechanical properties of Mg–RE alloys [5–10].

It is reported that $Mg_{97}Zn_1Y_2$ alloy prepared by rapidly solidified powder metallurgy (RS P/M) exhibits excellent properties, which possesses yield strength of 610 MPa and an elongation of 5% [11,12]. The improvement of the properties can be attributed to the ultra fine grains with average grain size of 200 nm and 18R and 14H type long period stacking ordered (LPSO) phases. In the $Mg_{89}Zn_4Y_7$ alloy composed mostly of LPSO phases [13,14], Hagihara et al. observed that (0 0 0 1) $\langle 1\,1\,\bar{2}\,0\rangle$ basal slip was the dominant operative deformation mode in LPSO phase and Schmid factor for basal slip was negligible when the stress was loaded along or normal to the (0 0 0 1) plane. Thus, the LPSO phase exhibits strong mechanical anisotropy. Furthermore, the type of LPSO phase had little influence on the operative deformation mode and the yield stress of the LPSO phase at ambient temperature [15]. Thus, by controlling the microstructure to achieve fine grain size and homogeneous dispersion of LPSO phase, the mechanical properties of the materials can be significantly improved.

Hot extrusion is a very effective technique to refine the microstructure and improve the mechanical properties of Mg alloys [16]. Extraordinary high-strength Mg–1.8Gd–1.8Y–0.7Zn–0.2Zr (at%) alloy exhibiting an ultimate tensile strength of 542 MPa, yield strength of 473 MPa and elongation to failure of 8.0% has been fabricated by indirect extrusion and subsequent ageing [17]. The improvement of the mechanical properties is attributed to the fine precipitates during ageing treatment and dynamic precipitation at the grain boundaries. In addition to high performance Mg alloy extrusion parts, high-strength Mg alloy sheets with good ductility are needed to extend the practical use of Mg alloys. Severe rolling (SR) process is an effective way to refine the microstructure and has potential to produce large Mg alloy sheets with ultra-fine grain size by industry due to the capacity of continuous production [18,19]. Due to the occurrence of significant grain refinement, the sheets are greatly strengthened and remarkably ductile [19]. However, there are few investigations on the preparation of Mg–Gd alloy sheets by severe rolling process [20,21]. Wang et al. reported that the Mg–12Gd–3Y–0.4Zr (wt%) alloy was hot rolled with total thickness reduction of 92% and the as-rolled sheet got the ultimate tensile

* Corresponding author. Tel.: +86 451 86402291; fax: +86 451 86413922.
E-mail address: zhenghe@hit.edu.cn (M.Y. Zheng).

0925-8388/$ – see front matter © 2012 Elsevier B.V. All rights reserved.
doi:10.1016/j.jallcom.2012.02.050

Table 1
Analyzed chemical composition of the ingot used in this study.

Element	Gd	Y	Zn	Zr	Mg
Weight%	8.23	3.83	1.02	0.35	Bal.
Atomic%	1.42	1.17	0.42	0.10	Bal.

strength of 382 MPa, tensile yield strength of 310 MPa and elongation to failure of 4.4% [21]. And the alloy was extruded before severe hot rolling process in order to improve the ductility and avoid the occurrence of cracking during rolling deformation [21], which increased the processing cost of the sheet. While the hot rolling was conducted directly to the cast Mg–Gd series alloys and usually the low-strain rolling process was adopted due to the low deformability of the cast alloys [22–24]. For example, in the rolling process of Mg–9Gd–4Y–0.4Zr (wt%) alloy [24], less than 10% reduction per pass and total reduction of 68% was introduced. Such a low amount of deformation cannot effectively refine the microstructure, leading to poor mechanical properties of the rolling sheet.

In the present study, severe hot rolling process with per pass reduction of 30–45% and total reduction of 96% was introduced to as-homogenized Mg–8.2Gd–3.8Y–1.0Zn–0.4Zr (wt%) alloy. Microstructure evolution and its effect on the mechanical properties of the alloy sheet were discussed.

2. Experimental

An ingot of Mg–Gd–Y–Zn–Zr alloy with 280 mm in diameter and 2940 mm in length was produced by semi-continuous casting method, and its chemical composition tested by inductive coupled plasma emission spectrometry (ICP) is shown in Table 1. Plates with the dimension of 150 mm × 100 mm × 30 mm were all cut from the center of the ingot, the same position can guarantee the same composition of each initial plates. The solution treatment was performed at 510 °C for 12 h, followed by an immediate warm water quench with the temperature of ~60 °C.

The solution treated plates were preheated at 400 °C for 30 min in the resistance furnace to homogenize the temperature of samples, meanwhile the mill roll was heated to 400 °C by the resistance heater. Then the hot rolling was performed with the initial thickness reduction of 20% and subsequent thickness reductions of 30–45%, which resulted in a total reduction of 96%. After each passes, the rolling samples were reheated at 400 °C for 10 min.

For the analysis of the microstructure evolution during hot rolling, optical microscope (OM) and JEOL JSM-7000F field-emission scanning electron microscope (FE-SEM) were performed on the samples with the total reduction from 60% to 96%. The samples were mechanical polished and then etched in the picric acid. The texture analysis was conducted by EDAX-TSL EBSD system operating at 25 kV, equipped with OIM Analysis software. Transmission electron microscope (TEM) was carried out in a FEI-TECNAI G^2 F30 operating at 200 kV. Thin foils for TEM observation were punched to discs of 3 mm in diameter, mechanically polished to ~50 μm and then ion-milled using Gatan plasma ion polisher.

The tensile specimens have a gauge length of 15 mm and cross-sectional areas of 6 mm × 1–2 mm were cut from the sheets by electrical discharge machining. Three directions were selected for tensile testing to examine the mechanical anisotropy of the rolling sheets: parallel to the rolling direction, inclined at an angle of 45° to the rolling direction and perpendicular to the rolling direction. The tensile tests were conducted at ambient temperature on an Instron 5569 testing machine with a cross-head speed of 1 mm/min.

3. Results and discussion

3.1. Microstructure evolution and texture examination

Fig. 1 shows the microstructure of the as-rolled sheets with different total reductions observed on the RD-ND plane. The average grain size of as-rolled sheet with 60% total reduction was more than 100 μm with the original $Mg_3(Gd,Y)$ eutectic phases around the deformed grains, and many twins intersected to each other were observed as shown in Fig. 1a. Meanwhile, because of the stress concentration near the eutectic phases, a "necklace" structure containing the fine dynamic recrystallization (DRX) grains was formed, as shown in the image with high magnification inserted in Fig. 1a. All of the deformed grains were mainly composed of plate-shaped long period stacking ordered (LPSO) phase. However, no plate-shaped LPSO phase was observed in the dynamic recrystallized region near the original grain boundaries. The LPSO phase mainly precipitated during the preheat treatment and the hot rolling process at 400 °C, because very few LPSO phase were observed in the as-homogenized sample before hot rolling. In addition, isolated block shaped phases were also observed inside some large grains.

With the increment of reduction ratio, the amount of twins diminished and disappeared after rolling with total reduction of 81% (Fig. 1b and c). Furthermore, the deformed grains were stretched along the rolling direction, especially near the shear bands and were broken up by the more and more shear bands formed with increasing reduction ratio, as shown in Fig. 1d–f. The original eutectic phases were broken and dispersed uniformly, and the volume fraction of DRX grains increased gradually with increasing reduction ratio. The as-rolled sheet with reduction ratio of 96% was almost fully recrystallized with average grain size of about 3.6 μm. In addition, with increasing volume fraction of recrystallized grains, the volume fraction of LPSO phase was

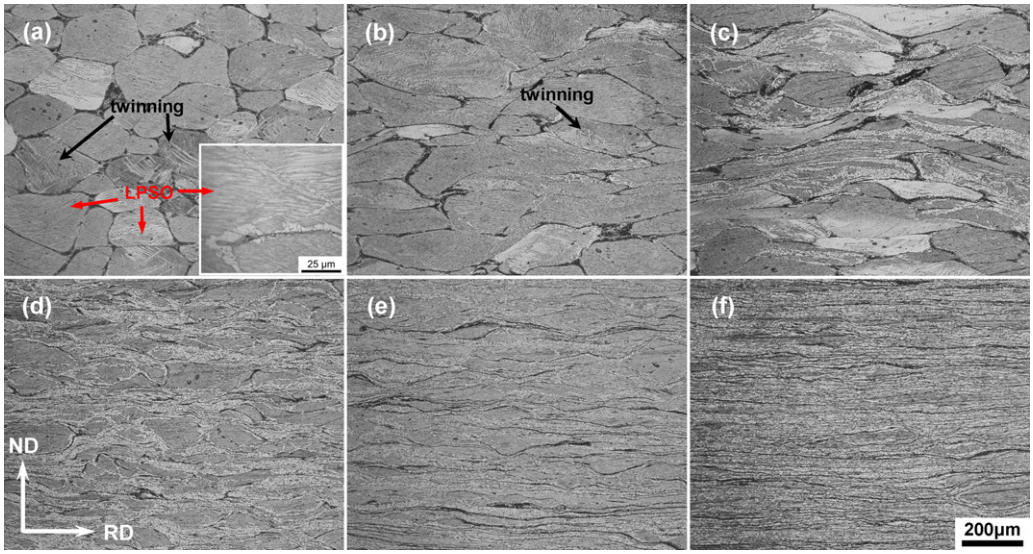

Fig. 1. Optical microstructures of the as-rolled sheet with different total reductions: (a) 60% (12 mm sheet), (b) 73% (8 mm sheet), (c) 81% (5.7 mm sheet), (d) 89% (3.3 mm sheet), (e) 93% (2.0 mm sheet), (f) 96% (1.2 mm sheet).

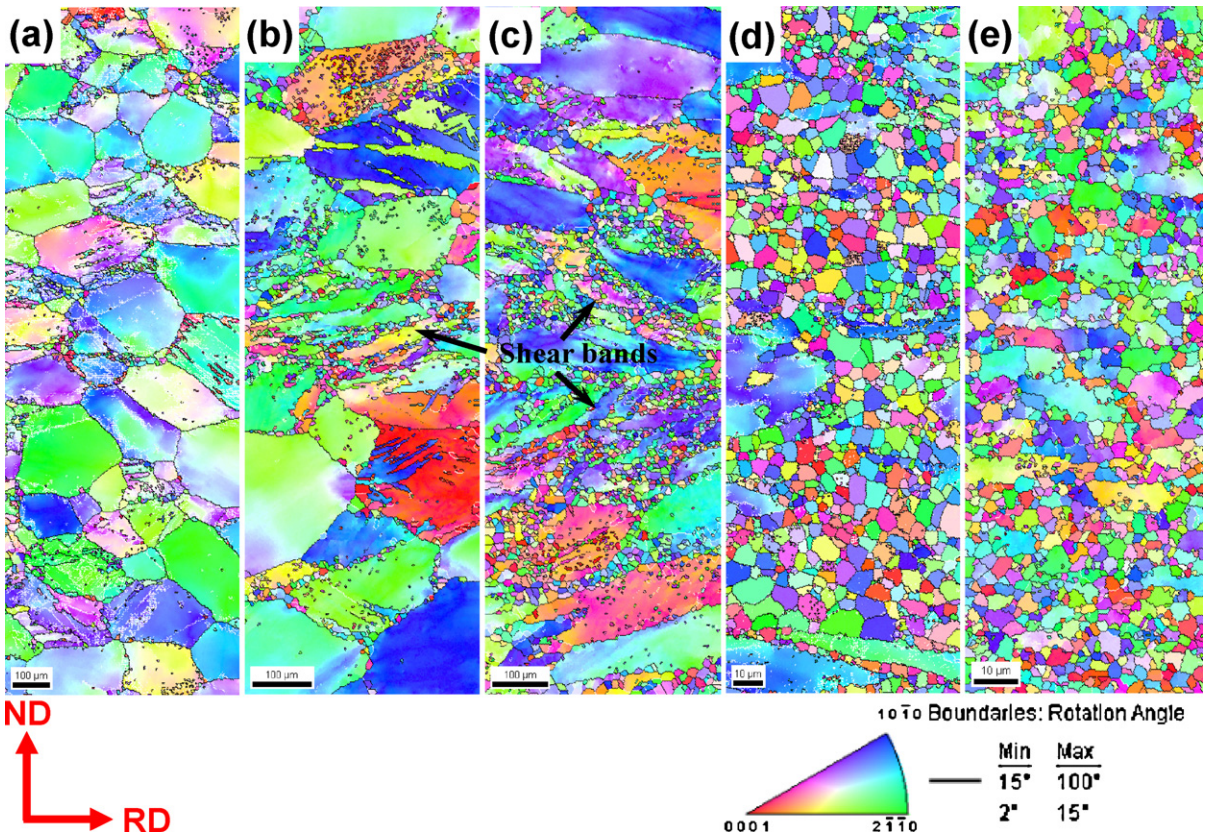

Fig. 2. EBSD orientation maps of sheets in the as-rolled condition with different total reduction: (a) 60% (12 mm sheet), (b) 73% (8 mm sheet), (c) 81% (5.7 mm sheet), (d) 89% (3.3 mm sheet), (e) 93% (2.0 mm sheet), (f) 96% (1.2 mm sheet).

decreased, and LPSO phase were not observed in the recrystallized grain. Similar phenomenon was reported by Chun et al. [25] in Mg–6Gd–1Zn–0.6Zr alloy processed by hot rolling, the LPSO phase were formed during hot rolling, while after annealing at 450 °C, the recrystallized grains were free of these plate shape precipitates. The LPSO phase were reorientated during hot rolling process to align along the rolling direction, as shown in Fig. 1

Fig. 2 shows EBSD orientation maps of the as-rolled samples with different reductions. It can be seen that a majority of the deformed grains had the orientation with prismatic plane parallel to the cross-sectional plane. For the deformed grains with *c*-axis nearly parallel to the ND, the basal slip was difficult to be activated due to the negligible Schmid factor when the stress was parallel to the basal plane, and $\{10\bar{1}2\}$ tensile twinning with lower activation energy compared with non-basal slip systems easily occurred [26]. Since twinning changed the orientation of the grains, the dislocations could glide in the twins and DRX occurred in these areas. Furthermore, the volume fraction of the recrystallized grains

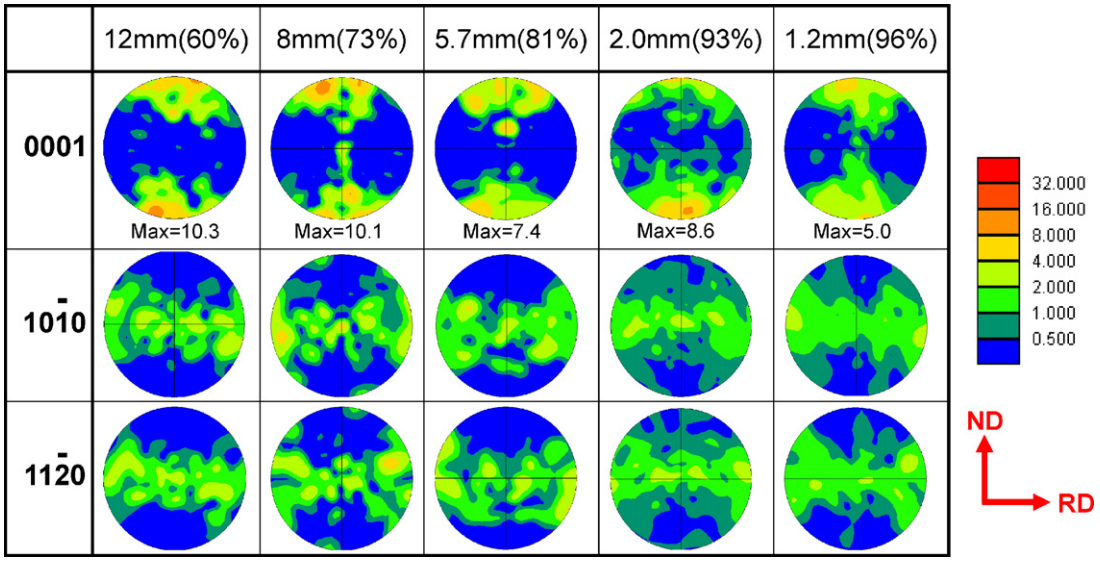

Fig. 3. Texture evolution of the as-rolled sheets with increasing total rolling reduction.

increased with increasing rolling passes, and almost fully recrystallized and homogeneous microstructure was obtained after final rolling (Fig. 2e and f).

Fig. 3 shows the texture evolution of the rolling sheet after different reduction ratio. Basal texture with the (0 0 0 1) basal plane of magnesium crystal parallel to the rolling plane was formed in all the as-rolled sheets. The samples with reduction from 60% to 81% exhibit texture with basal poles spreading from normal direction toward rolling direction. In the present study, the intensity of the basal texture decreased gradually with increasing rolling reduction ratio. The peak of the basal pole intensity tilted slightly from ND to TD and the basal poles in all samples texture showed a broad distribution towards RD and TD especially in the sheet with 96% reduction. It is generally accepted that rare earth elements can weaken the basal texture of Mg alloys [27–31]. Bohlen et al. analyzed the influence of rare earth element on the texture and anisotropy of the as-rolled Mg–Zn–RE sheets [27] and reported that the addition of Y led to a weakening of the texture and made the basal poles spread greater toward TD than RD. Al-Samman et al. also investigated the effect of rare earth elements on the texture modification in Mg–Zn–Zr–RE alloy sheets prepared by hot rolling [29] and they suggested that Gd modified the rolling texture most efficiently and showed a peak basal pole intensity of 4 multiples of a random distribution located at ~40° from ND to TD, and significant improvement in ambient temperature ductility and planar anisotropy was obtained. However, there is still a debate regarding the mechanism of texture weakening by addition of RE elements. The main reasonable mechanisms were particle stimulated nucleation (PSN) of recrystallization [30,31], shear band nucleation [28] and solute drag effect [29]. The rare earth element content of the alloy used in the present research was 8.2 wt% Gd and 3.8 wt% Y, which was much higher than those in the researches above mentioned [27–29]. Thus the high rare earth content and mixed addition resulted in the precipitation of large amount of the second phases in the alloy and distributed both along the grain boundaries with the block shape and inside the grains with plate shape. Such precipitates can hinder the movement of the dislocations so that the stress could concentrate easily near the precipitates, which promoted the dynamic recrystallization then weaken the basal texture. The volume fraction of the DRX grains increased gradually with increasing reduction ratio, this may led to the decrement of the intensity of the basal texture. In addition, Gd and Y elements with large atom radius had high solid solubility in Mg matrix [32,33], because these solute atoms were prone to segregate at the grain boundaries to decrease the free energy, they significantly affected the grain boundary migration rate. This could also be a rational factor for generating a random orientation [29].

Fig. 4a shows the bright-field TEM image of the eutectic phases on the original grain boundaries in the as-rolled sheet with 89% total reduction. Fig. 4b and c shows the selected area electron diffraction (SAED) patterns taken from regions marked with B and C in Fig. 4a, respectively. Fig. 4d supplies the data of EDX analysis of the region marked with B to identify the phase. The results demonstrate that the phases distributed along the original grain boundaries had face-centered cubic structure and had an average composition of Mg–16.9Gd–8.8Y–3.0Zn (at%), so they should be $(Mg,Zn)_3(Gd,Y)$ [34,35]. In the SAED patterns shown in Fig. 4c obtained from plate-shaped phases marked C in Fig. 4a, the distance between the incident beam spot and (0 0 0 2) matrix spot was divided into 18 equal intervals, which indicated the LPSO phase was 18R type. Meanwhile, five parallel weak streaks aligned along [0 0 0 1] direction between incident beam spot and $(1\,1\,\bar{2}\,0)$ fundamental spot of the magnesium matrix with equal distance. Similar phenomenon was reported in Mg–Zn–Y and Mg–Zn–Gd alloys [36–38]. Zhu et al. reported that [38] 18R-type LPSO had an ordered base-centered monoclinic structure and the stacking sequence of the closely packed plane was ABABCACACABCBCBCABA. In such model of the 18R unit cell, two middle layers in each ABCA-type block had an ordered arrangement of Y and Zn atoms, which caused the diffraction patterns containing the streaks along the [0 0 0 1] [38]. During heat treatment among the adjacent rolling processes and during hot rolling processes at 400 °C, the solubility of the rare earth elements increased and the mobility of the solute atoms was activated. Thus the rare earth atoms diffused from

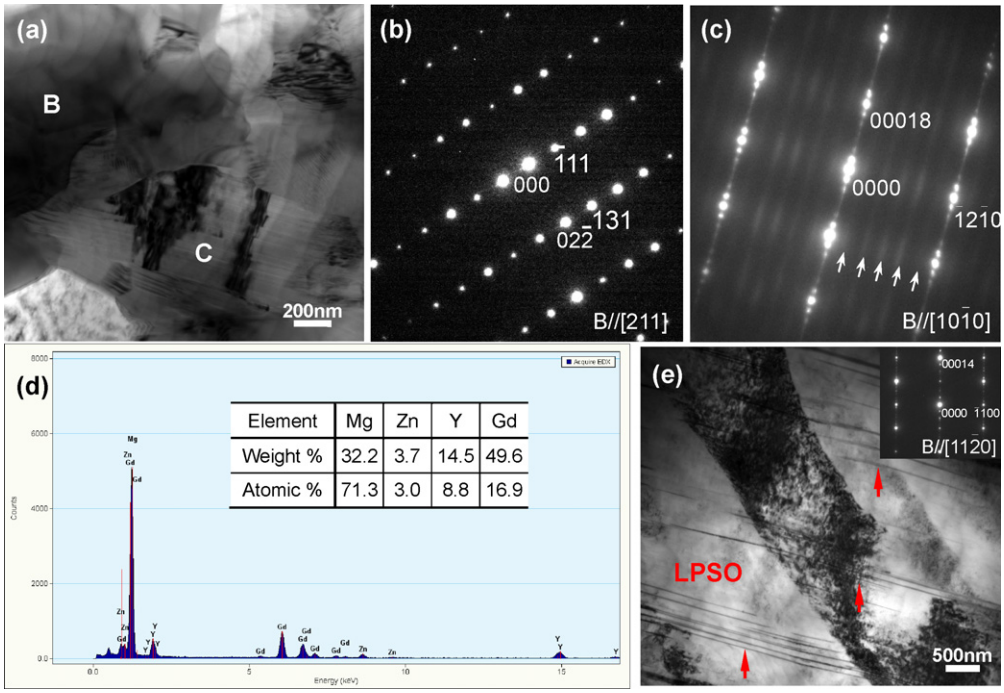

Fig. 4. (a) Bright-field image of the as-rolled sheet with 89% total reduction (3.3 mm), (b) and (c) SAED patterns of the regions marked B and C in (a), respectively, (d) EDS data from the phase marked B in (a), (e) bright-field image of the LPSO phase in the sheet and its corresponded SAED patterns.

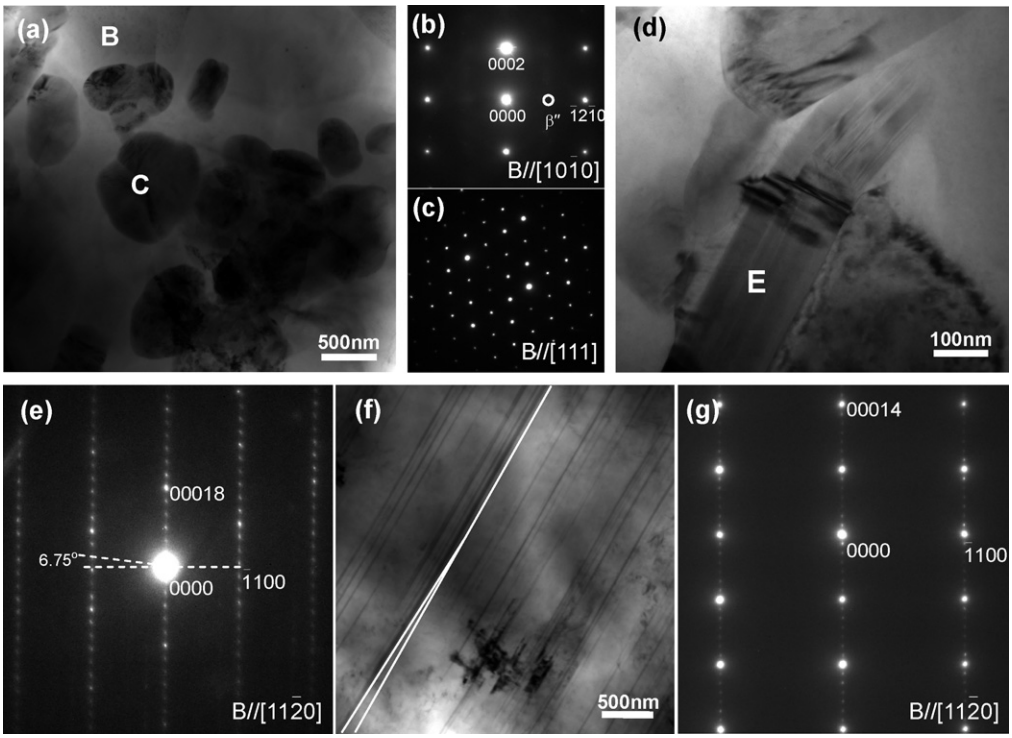

Fig. 5. (a) Bright-field image of the as-rolled sheets with 96% total reduction (1.2 mm), (b) and (c) SAED patterns of the grain marked B and phase marked C in (a), respectively, (d) and (f) bright-field image of the LPSO phase near and far from the block shaped phases, respectively, (e) SAED patterns of the region marked E in (d), (g) SAED patterns of (f).

the grain boundaries to the interior of the grains, which caused the concentration of the eutectic phases declined and phases dissolved, then LPSO phase precipitated in these areas with relative high concentration of RE elements.

The bright-field TEM image of the LPSO phase inside the grain was shown in Fig. 4e. The morphology of the LPSO phase inside the grain was obviously different from that at the grain boundaries. According to the SAED pattern with electron beam//[1 1 $\bar{2}$ 0] corresponding to the LPSO phase in Fig. 4e, they were 14H-type LPSO phase due to the distance from incident beam spot to the 0 0 0 2 magnesium matrix spot was divided into 14 parts. Because the concentration of Zn and rare earth elements near the grain boundaries was much higher than that inside the grains, the density of the LPSO phase precipitated at the grain boundaries was higher than those inside the grains. Furthermore, lots of dislocations were observed to slide across the LPSO phase, where the LPSO phase were bended, as shown in Fig. 4e, due to the stress concentration resulted from the impedance of dislocation movement by the LPSO phase.

Fig. 5a reveals the bright-field TEM micrograph of the sheet with 96% total reduction. It can be seen that the some ellipsoidal submicron sized particles distributed at the grain boundaries. The particle marked with C was identified to be equilibrium β phase (Mg_5(Gd,Y), face-centered cubic structure, F-43m, a = 2.23 nm [39]). The β phase heterogeneously precipitated at the grain boundaries due to the dynamic precipitation during hot wrought process [40], and the dynamic precipitation progress was significantly improved by deformation [41]. In addition, fine precipitates were dispersed densely inside the grains, as shown in Fig. 5a. The presence of extra diffraction spots at $1/2(1\,1\,\bar{2}\,0)_\alpha$ in the SAED pattern (Fig. 5c) demonstrated that these precipitates were β″ phases with definite crystallographic orientation relationship with the matrix, that is $(1\,1\,\bar{2}\,0)_{\beta''}//(1\,1\,\bar{2}\,0)_\alpha$ and $[0\,0\,0\,1]_{\beta''}//[0001]_\alpha$. It is reported that the precipitation of coherent β″ phase was not affected by dislocation density introduced by deformation [42], thus the precipitates were formed from interior of the supersaturated α-Mg matrix during subsequent cooling process in the air after final rolling with 40% reduction.

Fig. 5d shows the bright-field TEM images of the LPSO phase at the grain boundaries. As shown in the corresponding SAED patterns of the LPSO phase, the presence of the extra diffraction spots at $1/6(0\,0\,0\,1)_\alpha$ positions and the tilt of (0 1 1 0) plan of the LPSO phase about 83° from c-axis of the hexagonal close-packed structure illustrated that the LPSO were 18R-type LPSO phases [38]. The morphology of these 18R-type LPSO phase was similar to that formed in sheets with total reduction of 89%, and they may also precipitate from the supersaturated solid solution due to the dissolution of $(Mg,Zn)_3(Gd,Y)$. Fig. 5f shows the bright-field TEM images of the LPSO phase inside the grains. The corresponding SAED patterns as shown in Fig. 5g indicates the LPSO phase was 14H LPSO. It was reported that the composition of 18R-type and 14H-type LPSO phase were $Mg_{10}YZn$ and $Mg_{12}YZn$, respectively, in Mg–Y–Zn alloy [38]. It suggests that the type of LPSO phase may depend on the concentration of Zn and rare earth elements, that is, 18R-type precipitated densely at the grain boundaries rich in Zn and rare earth atoms, while 14H-type precipitated inside the grains with low concentration of solute atoms.

The 14H-type LPSO phase were bended as shown in Fig. 5f, same phenomenon was also observed in the sheet with 89% reduction, as shown in Fig. 4e. Because the operative deformation mode in LPSO phase was basal slip, non-basal slip across the LPSO phase would significantly be restricted and the stress concentration occurred near the LPSO phase. The bend of these phases can accommodate the local strain then improved the ductility and strength of the alloy sheets [43].

3.2. Mechanical properties

The stress–strain curves along RD of the as-rolled sheets with different total reductions at ambient temperatures were plotted in Fig. 6, and the corresponding ultimate tensile strength (UTS), tensile

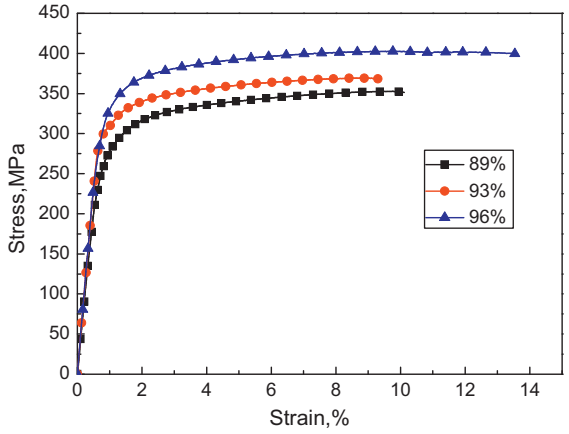

Fig. 6. Tensile properties of the as-rolled sheets with different total reductions tested along RD at ambient temperature.

yield strength (TYS) and elongation to failure were also summarized in Table 2. The presented data clearly reveals that the UTS and TYS were obviously improved with increasing rolling reductions and UTS of 403 MPa, TYS of 318 MPa and elongation of 13.7% were obtained after total rolling reduction of 96%. The enhancement of the strength should attribute to several factors. Firstly, since the average grain sizes decreased gradually with the increasing rolling reductions and refined to approximately 3.6 μm after final rolling (Fig. 1f), according to Hall–Petch relationship such fine grains may improve the proof strength. On the other hand, the composition of the alloy with high rare earth elements were selected in the present research, which resulted in enrichment of solute atoms in the grains and precipitation of numerous phases at the grain boundaries. The phases at the grain boundaries became the obstacles for the motion of the dislocations and then the stress concentration occurred. Additionally, the stress concentration near the phases promoted the dynamic recrystallization and refined the microstructure. Furthermore, most of the LPSO phase observed in the sheets aligned along the rolling direction suggesting that the interfaces between the LPSO phase and the Mg matrix were inclined to the tensile axis with negligible Schmid factor for $(0\,0\,0\,1)\langle 1\,1\,\bar{2}\,0\rangle$ basal slip at room temperature. Thus, the shear deformation mainly occurred through the LPSO phase with the plate shape when the force loading along the RD and which acted as fiber reinforcement for the alloy [43]. Because of the precipitation of fine and dense β″ phases in the sheet with 96% total reduction (Fig. 5a), the proof strength was further improved compared with other samples. The elongation to failure of the sample after final rolling reached 13.7% along the RD. The improvement of ductility was mainly due to the much more homogeneous microstructure and the fine recrystallized grains. The refined grain sizes obviously shorten the distance of dislocations slip and then released the dislocation pile-up.

Table 2
Tensile properties of the Mg–8Gd–4Y–1Zn–0.4Zr alloy under different conditions.

Status	Orientation	UTS (MPa)	YTS (MPa)	Elongation (%)
3.3 mm sheet	RD	353	263	10.2
	45°	323	239	10.5
	TD	312	233	6.0
2.0 mm sheet	RD	370	305	9.4
	45°	347	257	8.1
	TD	333	251	5.5
1.2 mm sheet	RD	403	318	13.7
	45°	380	283	14.5
	TD	371	270	13.5

The mechanical properties of the samples measured along three tensile directions RD, 45° and TD were summarized in Table 2. In the hot rolling process of common magnesium alloys without rare earth elements, the highest proof strength was obtained in the TD and lowest in the RD with basal poles tilted to the RD [44]. However, in the present study, the samples tested along the RD exhibited superior yield and ultimate tensile strength than those along the 45° and TD. Additionally, the difference between RD and 45° was much more pronounced than that between 45° and TD, similar results were obtained in other RE containing magnesium alloys [27]. This is resulted from the texture development in the as-rolled sheets with broader distribution of basal poles towards the TD than the RD. As a consequence, the grains with the c-axis inclined from the ND to the TD were favorable for the basal slip and tensile twinning with higher Schmid factor when the force loaded along the TD. The anisotropy of the strength and elongation was improved with increasing rolling reduction, and the distinction among the different tensile directions in the sample with 96% reduction was less obvious. One possible reason was the weakened texture with broader spread and lower peak intensity of the basal poles. Furthermore the high volume fraction of the recrystallization also contributed to the good elongation of the sample tested along the TD.

4. Conclusions

The microstructure evolution and mechanical properties of Mg–8.2Gd–3.8Y–1.0Zn–0.4Zr alloy sheet were analyzed and the results were summarized as follows:

1. The dynamic recrystallization was apt to occur near the phases at the grain boundaries and the deformation twins because of the stress concentration and. The twins disappeared after severer rolling and the microstructure almost fully recrystallized after rolling with 96% total reduction.
2. Although all the as-rolled sheets exhibited a typical basal texture with the basal plane parallel to the rolling plane, the intensity of the texture was significantly weakened by the addition of rare earth elements and recrystallization. The spread of the basal poles were greater toward the TD than the RD in all samples.
3. The LPSO phase at the grain boundaries and inside the grains had different structure: 18R type LPSO phase located at the grain boundaries and 14H type LPSO phase distributed inside the grains.
4. The sheets after rolling with total reduction of 96% exhibited excellent mechanical properties with UTS of 403 MPa, TYS of 318 MPa and elongation to failure of 13.7%, and anisotropy of the strength and elongation was improved with increasing rolling reduction.

Acknowledgments

This work is supported by the International Cooperation Key Project supported by Ministry of Science and Technology (MOST), China (2010DFB50210) and Project of Scientific Researchers Serving for Enterprises supported by Ministry of Science and Technology, China (2009GJB20003).

References

[1] A.K. Dahle, Y.C. Lee, M.D. Nave, P.L. Schaffer, D.H. John, J Light Met. 1 (2001) 61–72.
[2] J.M. Kim, K. Shin, K.T. Kim, W.J. Jung, Scr. Mater. 49 (2003) 687–691.
[3] X.F. Huang, W.Z. Zhang, J.F. Wang, W.W. Wei, J. Alloys Compd. 516 (2012) 186–191.
[4] L.X. Hu, H. Wang, X. Wang, J. Alloys Compd. 513 (2012) 343–346.
[5] J.F. Nie, K. Oh-ishi, X. Gao, K. Hono, Acta Mater. 56 (2008) 6061–6076.

[6] J. Grobner, R. Schmid-Fetzer, J. Alloys Compd. 320 (2001) 296–301.
[7] J.F. Nie, X. Gao, S.M. Zhu, Scr. Mater. 53 (2005) 1049–1053.
[8] Y. Liu, G.Y. Yuan, W.J. Ding, C. Lu, J. Alloys Compd. 427 (2007) 160–165.
[9] B.L. Xiao, Q. Yang, J. Yang, W.G. Wang, G.M. Xie, Z.Y. Ma, J. Alloys Compd. 509 (2011) 2879–2884.
[10] M. Pekguleryuz, M. Celikin, M. Hoseini, A. Becerra, L. Mackenzie, J. Alloys Compd. 510 (2012) 15–25.
[11] Y. Kawamura, K. Hayashi, A. Inoue, T. Masumoto, Mater. Trans. JIM 42 (2001) 1172–1176.
[12] A. Inoue, Y. Kawamura, M. Matsushita, K. Hayashi, J. Koike, J. Mater. Res. 16 (2001) 1894–1900.
[13] K. Hagihara, A. Kinoshita, Y. Sugino, M. Ymasaki, Y. Kawamura, H.Y. Yasuda, Y. Umakoshi, Intermetallics 18 (2010) 1079–1085.
[14] K. Hagihara, N. Yokotani, Y. Umakoshi, Intermetallics 18 (2010) 267–276.
[15] K. Hagihara, N. Yokotani, A. Kinoshita, Y. Sugino, H. Yamamoto, M. Ymasaki, Mater. Res. Soc. Proc. 1128 (2009) U05–U53.
[16] K. Liu, J. Meng, J. Alloys Compd. 509 (2011) 3299–3305.
[17] T. Honma, N. Kunito, S. Kamado, Scr. Mater. 61 (2009) 644–647.
[18] J.A. del Valle, O.A. Ruano, Mater. Lett. 63 (2009) 1551–1554.
[19] M.T. Perez-Prado, J.A. del Valle, O.A. Ruano, Mater. Lett. 59 (2005) 3299–3303.
[20] A. Muller, G. Garces, P. Perez, P. Adeva, J. Alloys Compd. 443 (2007) L1–L5.
[21] R. Wang, J. Dong, L.K. Fan, P. Zhang, W.J. Ding, Trans. Nonferrous Met. Soc. China 18 (2008) s189–s193.
[22] D. Wu, R.S. Chen, E.H. Han, J. Alloys Compd. 509 (2011) 2856–2863.
[23] J. Geng, Y.B. Chun, N. Stanford, C.H.J. Davies, J.F. Nie, M.R. Barnett, Mater. Sci. Eng. A 528 (2011) 3659–3665.
[24] L. Li, X.M. Zhang, Y.L. Deng, C.P. Tang, J. Alloys Compd. (2009) 295–299.
[25] Y.B. Chun, J. Geng, N. Stanford, C.H.J. Davies, J.F. Nie, M.R. Barnett, Mater. Sci. Eng. A 528 (2011) 3653–3658.
[26] T. Al-Samman, G. Gottstein, Mater. Sci. Eng. A 490 (2008) 411–420.
[27] J. Bohlen, M.R. Nurnberg, J.W. Senn, D. Letzig, S.R. Agnew, Acta Mater. 55 (2007) 2101–2112.
[28] N. Stanford, M.R. Barnett, Mater. Sci. Eng. A 496 (2008) 399–408.
[29] T. Al-Samman, X. Li, Mater. Sci. Eng. A 528 (2011) 3809–3822.
[30] E.A. Ball, P.B. Prangnell, Scr. Metall. Mater. 31 (1994) 111–117.
[31] G.W. Lorimer, L.W.F. Mackenzie, F.J. Humphreys, T. Wilks, Mater. Sci. Forum 488–489 (2005) 99–102.
[32] L. Gao, R.S. Chen, E.H. Han, J. Alloys Compd. 481 (2009) 379–384.
[33] Y. Gao, Q.D. Wang, J.H. Gu, Y. Zhao, Y. Tong, Mater. Sci. Eng. A 459 (2007) 117–123.
[34] M. Yamasaki, M. Sasaki, M. Nishijima, K. Hiraga, Y. Kawamura, Acta Mater. 55 (2007) 6798–6805.
[35] S. Zhang, G.Y. Yuan, C. Lu, W.J. Ding, J. Alloys Compd. 509 (2011) 3515–3521.
[36] E. Abe, Y. Kawamura, K. Hayashi, A. Inoue, Acta Mater. 50 (2002) 3845–3857.
[37] K. Saito, A. Yasuhara, K. Hiraga, J. Alloys Compd. 509 (2011) 2031–2038.
[38] Y.M. Zhu, A.J. Morton, J.F. Nie, Acta Mater. 58 (2010) 2936–2947.
[39] M.L. Fornasini, P. Manfrinetti, Acta Crystallogr. C 42 (1986) 138–141.
[40] X.L. Hou, Z.Y. Cao, L.D. Wang, S.W. Xu, S. Kamado, L.M. Wang, Mater. Sci. Eng. A 528 (2011) 7805–7810.
[41] H. Beladi, M.R. Barnett, Mater. Sci. Eng. A 452–453 (2007) 306–312.
[42] J. Cizek, I. Prochazka, B. Smola, I. Stulikova, V. Ocenasek, J. Alloys Compd. 430 (2007) 92–96.
[43] K. Hagihara, A. Kinoshita, Y. Sugino, M. Yamasaki, Y. Kawamura, H.Y. Yasuda, Y. Umakoshi, Acta Mater. 58 (2010) 6282–6293.
[44] Y. Chino, K. Sassa, A. Kamiya, M. Mabuchi, Mater. Sci. Eng. A 441 (2006) 349–356.